Research Article

Shaobo Li, Shuming Yang*, Fei Wang, Qiang Liu, Biyao Cheng and Yossi Rosenwaks

Plasmonic interference modulation for broadband nanofocusing

https://doi.org/10.1515/nanoph-2021-0405
Received July 25, 2021; accepted October 14, 2021;
published online October 26, 2021

Abstract: Metallic plasmonic probes have been successfully applied in near-field imaging, nanolithography, and Raman enhanced spectroscopy because of their ability to squeeze light into nanoscale and provide significant electric field enhancement. Most of these probes rely on nanometric alignment of incident beam and resonant structures with limited spectral bandwidth. This paper proposes and experimentally demonstrates an asymmetric fiber tip for broadband interference nanofocusing within its full optical wavelengths (500–800 nm) at the nanotip with 10 nm apex. The asymmetric geometry consisting of two semicircular slits rotates plasmonic polarization and converts the linearly polarized plasmonic mode to the radially polarized plasmonic mode when the linearly polarized beam couples to the optical fiber. The three-dimensional plasmonic modulation induces circumference interference and nanofocus of surface plasmons, which is significantly different from the nanofocusing through plasmon propagation and plasmon evolution. The plasmonic interference modulation provides fundamental insights into the plasmon engineering and has important applications in plasmon nanophotonic technologies.

Keywords: asymmetric slits; broadband nanofocusing; circumference interference; plasmonic modulation; polarization rotation.

***Corresponding author: Shuming Yang**, State Key Laboratory for Manufacturing Systems Engineering, Xi'an Jiaotong University, Xi'an 710049, Shaanxi, China, E-mail: shuming.yang@mail.xjtu.edu.cn. https://orcid.org/0000-0001-7685-537X
Shaobo Li, Fei Wang, Qiang Liu and Biyao Cheng, State Key Laboratory for Manufacturing Systems Engineering, Xi'an Jiaotong University, Xi'an 710049, Shaanxi, China
Yossi Rosenwaks, School of Electrical Engineering, Tel-Aviv University, Tel-Aviv 69978, Israel

1 Introduction

Surface plasmon polaritons (SPPs), the collective oscillation of electrons at the metal–dielectric interface, can intrinsically carry optical energy into the nanoscale without suffering from the diffraction limits [1, 2]. The nanofocusing characteristics of the SPP enabling confinement and enhancement of electromagnetic fields within nanoscale volumes have resulted in a variety of metallic structures that can modulate the propagation of SPP, such as metallic cones [3–5], metal-coated dielectric tapers [6, 7], wedges [8, 9], and nanogaps [10]. These plasmon engineerings on chip-based nanophotonic waveguides and three-dimensional enhanced nanofocusing have been applied to photonics integrated circuits [11–14], modulators [15–17], near-field super-resolution imaging [18–22], and nonlinear spectroscopy [23, 24].

The combination of SPP mode modulation and tapered metallic waveguides has led to many optical probes with excellent performance in near-field scanning optical microscopy (NSOM) and tip-enhanced Raman spectroscopy [25, 26]. In these applications, the metal-coated fiber tip [7, 27, 28] and nanograting-coupled tapered probes [29, 30] can realize nanofocusing with a large near field enhancement illuminated by radially polarized light because of the constructive interference of SPP waves [20, 25–30]. However, the generation of a radially polarized beam requires particularly complex processes, and the radially polarized excitation is sensitive to nanometric misalignments. To relieve these particular requirements, asymmetric metallic probes [31–37] have been demonstrated numerically and experimentally to converge plasmons to a nanoscale spot at the apex with linearly polarized light. Most of these cases generated and focused SPP waves on only one side of the probe [31, 34–36], which depends on plasmon propagation and scales down the near field enhancement. Additionally, only one resonance wavelength can obtain a better nanofocusing performance [34, 38–40], which limits the generation of broadband nanolight sources [35, 36]. Although three dimensional plasmonic nanofocusing has been demonstrated [32], direct radiation on the tip apex and spectrally narrow band limit its application. The combination

of large near field enhancement, broadband nanofocusing, and a background without noise is still a challenge for photonic sensing and imaging.

In this paper, an asymmetric fiber tip is introduced and experimentally demonstrated for the broadband delivery of light to nanoscale dimensions on a metallic nanotip, having an apex size of 10 nm, within its full optical wavelengths. The asymmetric structure consists of two semicircular slits on opposing facets of the tip, which will rotate plasmonic polarization and transform the linearly polarized SPP mode to the radially polarized SPP mode when the linearly polarized light focuses and couples to the asymmetric fiber. The experiments demonstrate that this three-dimensional plasmonic interference modulation induces broadband nanofocusing at the tip apex within the full optical wavelengths of the fiber because of the constructively circumference interference of SPP waves under broadband spectrum. The broadband interference nanofocusing could provide for multiple applications, including sensing, imaging, and nonlinear spectroscopy.

2 Results and discussion

2.1 Plasmonic probe design

A schematic of the asymmetric fiber tip for broadband nanofocusing is shown in Figure 1a. In this scheme, the linearly polarized light couples to the optical fiber and propagates in the HE_{11} waveguide mode. When passing through the two asymmetric semicircular slits, the linearly polarized SPP mode is excited and its polarization is then reversed, resulting in that the linearly polarized SPP mode (HE_{11}-SPP) is converted to the radially polarized SPP mode (TM_{01}-SPP), as shown in Figure 1b and c. With the decrease of fiber radius, the TM_{01}-SPP mode will not cut off, leading to constructive interference and a nanoscale spot at the tip apex (Figure 1d). Here, the HE_{11}-SPP and the TM_{01}-SPP denote corresponding SPP mode on surface of the metallized optical fiber excited by the linearly polarized mode (HE_{11}) and radially polarized mode (TM_{01}) in the optical fiber, respectively. Based on this mechanism, an asymmetric fiber tip is designed and its diagram and the scanning electron micrograph (SEM) are shown in Figure 1e and f. The asymmetric fiber tip was fabricated by tube-etching method first, which can obtain tapered fibers with uniformly cone angle of 32° under proper experimental conditions. To achieve tip apex below 10 nm, the gold was vertically evaporated on the tapered optical fiber and its thickness is 180 nm that can prevent unwanted transmitted light. Two asymmetric semicircular silts with width of 120 nm were then processed on the opposing facets of the metallic fiber tip by focused ion beam method to enable nanofocusing with linearly polarized light (also see Supplementary Figures S1 and S2), and they have an asymmetric degree of H = 935 nm (phase delay) that conforms to the circumference interference condition of SPP waves, determined by Eq. (1), causing plasmons excitation and modulation. The "circumference interference" here means that the interference of the SPP waves occurs around the entire solid circumference of the cone, and a constant phase difference is obtained at any two antipodal points of the circumference.

$$\Delta\Phi_L - \Delta\Phi_R = (2N-1)\pi \tag{1}$$

where $\Delta\Phi_L$ and $\Delta\Phi_R$ are phase delays in the optical fiber and on the surface of tapered metallic waveguide respectively. $\Delta\Phi_L = 2\pi \cdot H/\lambda_{OM}$, $\Delta\Phi_R = 2\pi \cdot [H/\cos(\theta/2)]/\lambda_{SPP}$, and $\lambda_{OM} = \lambda_0/n_{OM}$, $\lambda_{SPP} = \lambda_0\sqrt{(\epsilon_{air}+\epsilon_m')/\epsilon_{air}\epsilon_m'}$. The terms n_{OM} and λ_{OM} represent the refractive index and the effective wavelength of the optical mode respectively. Terms λ_0 and λ_{SPP} are the wavelength of the incident light and the SPP waves of Au/air interface, respectively. N is an integer. The terms ϵ_m and ϵ_{air} represent the dielectric constants of the Au film and surrounding medium respectively.

2.2 Nanofocusing mechanism of the asymmetric fiber tip

To explore the nanofocusing performance of this asymmetric fiber tip, detailed numerical analysis was calculated by the finite-difference time-domain (FDTD) method. The structure parameters of cone angle θ, slit width w and tip apex r are the same as that of the fabricated fiber tip (Figure 1e and f). Figure 2 compares the electric field distributions and phase maps in vicinity of the apex of symmetric and asymmetric fiber tips under linearly polarized light. When the linearly polarized light couples to the symmetric fiber tip [42–44], the HE_{11}-SPP mode is excited and becomes a leaky and unbound mode at the tip apex, which indicates that the polarization and the phase distribution of the SPP mode perfectly match that of the incident light in this case. Therefore, the HE_{11}-SPP mode has a reverse E_z phase distribution and the linear polarization, as shown in Figure 2a–c. While the TM_{01}-SPP mode has the same E_z phase distribution and the radial polarization, which is the only mode without cutoff [41–45] and can be effectively focused on the apex (Figure 1d). For the HE_{11}-SPP mode, the phases of line ① and line ② are reversal (Figure 2c). There is a π phase delay between the SPP waves at any two antipodal points of the circumference of the conical fiber tip, as shown in Figure 2d, where

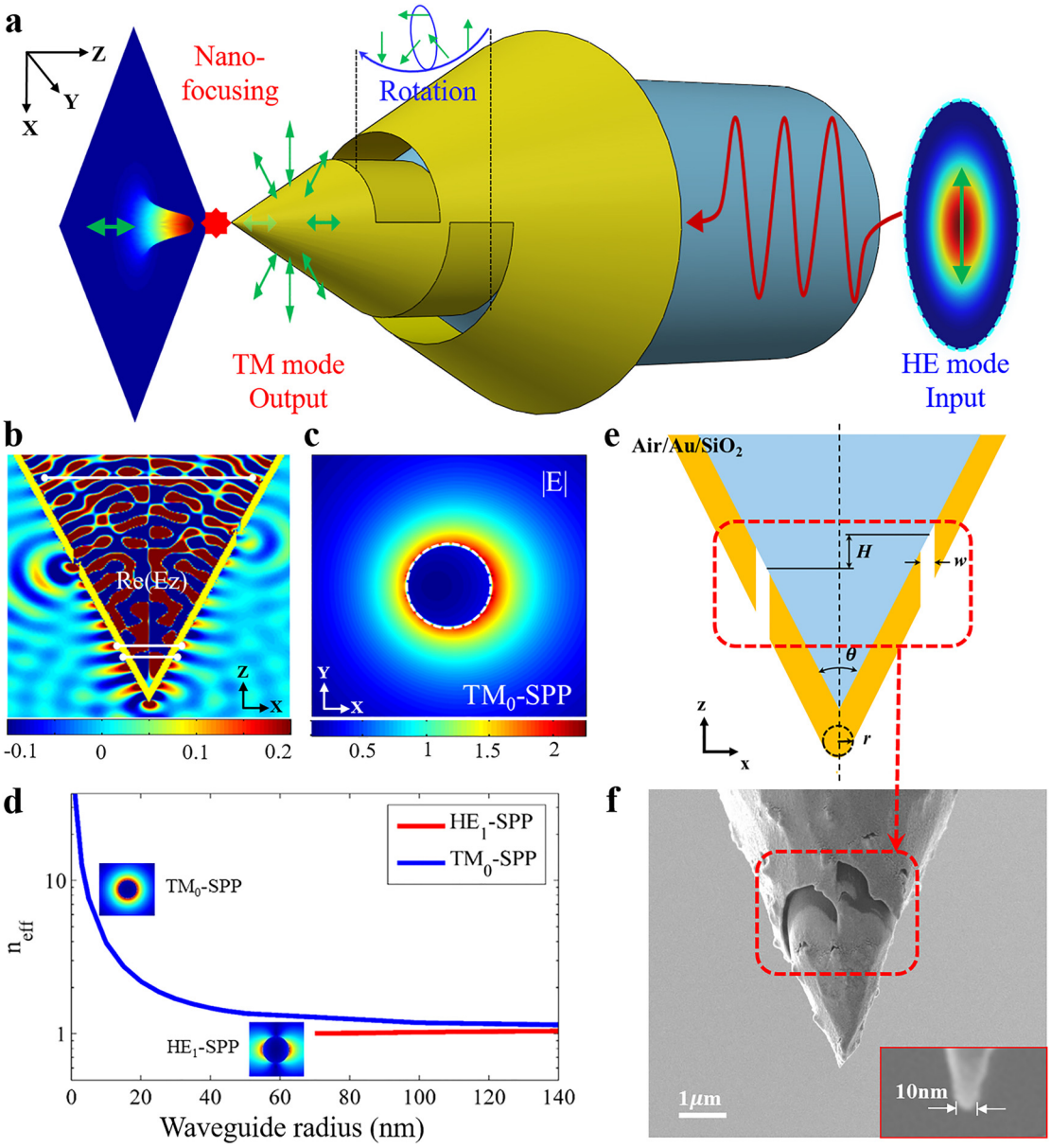

Figure 1: The asymmetric fiber tip for nanofocusing.
(a) Schematic of plasmon nanofocusing of the asymmetric fiber tip using internal illumination. When the linearly polarized mode (HE_{11}) with *X* polarization internally couples to the fiber, the HE_{11}-SPP modes are excited and modulated by the two asymmetric semicircular slits. Approaching the tip apex, the HE_{11}-SPP waves (b) reverse the polarization and (c) transform to the TM_{01}-SPP mode, displaying constructively circumference interference and forming a nanoscale spot at the tip apex. The white lines indicate the incident mode with reverse polarization (phase) and the SPP waves at any two antipodal points with same polarization (phase). (d) Calculated effective indices of the HE_{11}-SPP mode and TM_{01}-SPP mode with decrease of conical waveguide radius. (e) The *XZ* section of the asymmetric fiber tip. *H* indicates the height difference of the opposing asymmetric slits. θ, *r* and *w* indicate cone angle, tip radius and slit width, respectively. (f) The fabricated asymmetric fiber tip with 10 nm apex.

the SPP waves on the opposing facets can be regarded as two independent beams of light that display destructive interference. Therefore, compensating the phase delay will reverse the polarization of the SPP waves on the opposing facets, as depicted in Figure 2e, and the HE_{11}-SPP mode can be transformed to the TM_{01}-SPP mode (Supplementary Figures S3 and S4), thus allowing constructive interference and a nanoscale spot at the tip apex.

The HE_{11}-SPP mode induced by the symmetric fiber tip should be removed because of the contribution of the unwanted background illumination around the tip, thus the metal thickness was set to be 180 nm to decrease the

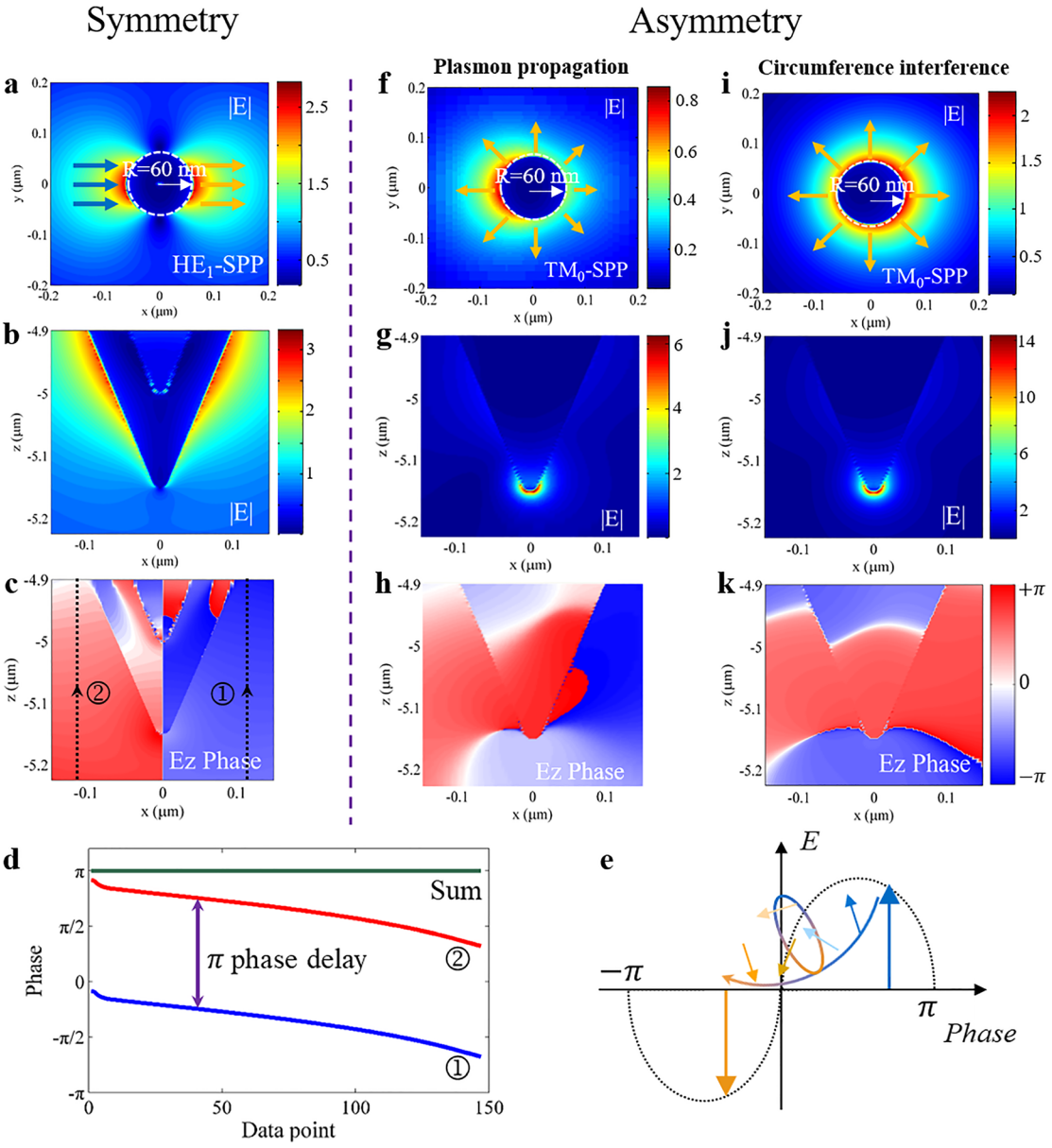

Figure 2: Nanofocusing comparison of symmetric and asymmetric fiber tips. The symmetric and asymmetric fiber tips are illuminated using a linearly polarized light at a wavelength of 633 nm. Electric field distribution of the HE_{11}-SPP mode on the (a) *XY* plane and on the (b) *XZ* plane excited by the symmetric fiber tip. The corresponding E_z phase distribution of the symmetric fiber tip on the (c) *XZ* plane. Electric field distribution of the TM_{01}-SPP mode on the (f) and (i) *XY* plane and on the (g) and (j) *XZ* plane excited by the asymmetric fiber tip. The corresponding E_z phase distribution of the asymmetric fiber tip on the (h) and (k) *XZ* plane. Panels (f)–(h) indicate nanofocusing through plasmon propagation and evolution, and panels (i)–(k) indicate the circumference interference plasmons nanofocusing. (d) Phase delay between the SPP waves on the opposing facets indicated in (c) and marked as ① and ②. The phases of line ① and line ② are reversed, and Sum = Phase ① + Phase ② = π. (e) The physical mechanism of polarization reversal of the SPP waves at any two antipodal points of the circumference. The size of the coordinate is scaled down to emphasize the electric field and phase distribution. The yellow and blue arrows indicate the electric field vector of the SPP waves on the opposing facet of the tip. The "symmetry" indicates no nanostructure on the conical Au film, while the "asymmetry" indicates one or two slits are etched on the Au film.

conversion efficiency of Kretschmann coupling [27, 33, 43] via the illumination of linearly polarized light (Supplementary S4). To get larger near field intensity, the orientation of asymmetric slits is parallel to the longitudinal direction of the fiber tip [41], in which the main energy flows to the apex (Supplementary Figure S1). With the design of asymmetric semicircular slits and the introduction of a π phase delay to the SPP waves at any two

antipodal points of the circumference, the asymmetric fiber tip achieved nanofocusing and strong electric fields confined at the tip apex, as displayed in Figure 2i–k. After phase delay, the HE_{11}-SPP mode is transformed to the TM_{01}-SPP mode (Figure 2i and j) with the same distributions as that in Supplementary Figure S3. Figure 2k shows that the E_z phase distribution of the circumference interference is the same on the opposing facets, which demonstrates the plasmonic nanofocusing is coupled to and enhanced by the constructive interference of SPP waves around the entire solid circumference of the cone. This phenomenon is different from the nanofocusing through plasmon propagation [35], i.e. one-side plasmonic excitation and nanofocusing. As shown in Figure 2f–h, the E_z phase distribution is reversed on the opposing facets and only the phase below the apex is the same because of one-side plasmon propagation and mode evolution near the apex (Supplementary Figure S9). Compared with one-side excitation method, the circumference interference method can confine light in the nanoscale, and converge larger local optical energy due to constructive interference and plasmonic nanofocusing of SPP waves.

2.3 Experiments of polarization nanofocusing

A linearly polarized light with the wavelength of 633 nm was focused and coupled to the optical fiber to investigate the plasmon nanofocusing and circumference interference characteristics of the fabricated asymmetric fiber tip, as shown in Figure 3a. The incident light power can be tuned by an attenuator (A), and the incident polarization can be continuously tuned by a half waveplate (HWP). The transmitted and scattered light were analyzed and imaged using a sensitive complementary metal oxide semiconductor (CMOS) camera.

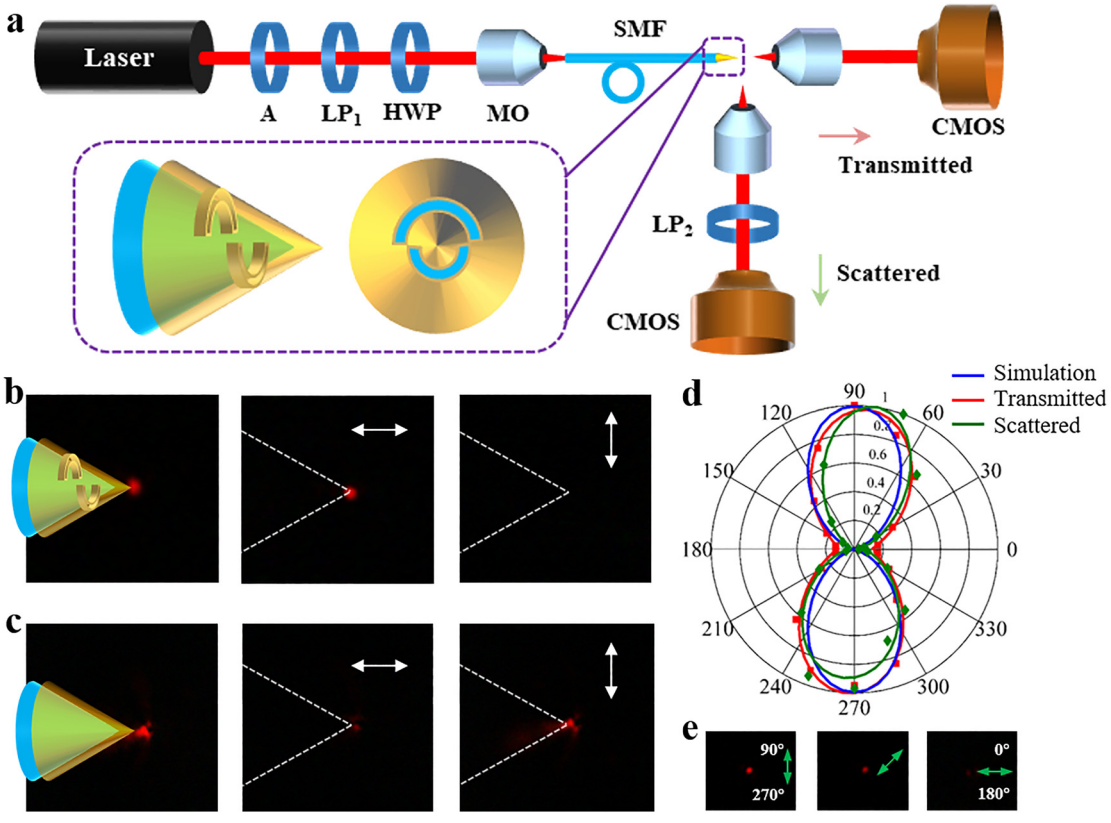

Figure 3: The experiments of plasmon nanofocusing.
(a) Schematic of the experimental setup. Optical images of the side-scattered light (b) of the asymmetric fiber tip and (c) of the symmetric fiber tip. The white arrows indicate the direction of the linear polarizer parallel or perpendicular to the tip axis. (d) Polar graph of the light spot intensity at the apex with respect to the incident polarization. (e) Optical images of the forward-transmitted light of the asymmetric fiber tip with respect to the incident polarization. The green arrows indicate the incident polarization. 90° and 270° correspond to the direction of incident polarization perpendicular to the boundary of the two asymmetric slits, i.e. incident mode with *X* polarization. 0° and 180° correspond to the direction of incident polarization parallel to the boundary of the two asymmetric slits, i.e. incident mode with *Y* polarization.
A: attenuator; HWP: half waveplate; CMOS: complementary metal oxide semiconductor; LP: linear polarizer; MO: micro-objective.

Figure 3b shows the scattered optical images of a fabricated asymmetric fiber tip with inserting a linear polarizer (LP_2) before camera. The white arrows indicate the direction of the LP_2 relative to the tip axis. A red light spot was clearly observed at the tip apex, which was the far-field radiation from the nanolight source. From these images, the side-scattered light is seen to be purely longitudinally polarized, implying that it results from plasmon nanofocusing. For a symmetric fiber tip (Figure 3c) with no slit and a gold film thickness of 90 nm, there is also a red light spot, but this side-scattered light is purely transversely polarized, further confirming that the scattering of longitudinal components in Figure 3b is induced by the plasmon nanofocusing, not from the leaked incident linearly polarized light.

The dependence of the intensity of the light spot on the polarization of incident light without LP_2 in front of camera was explored to further verify that the light spot was associated with asymmetric geometry and plasmon nanofocusing. In Figure 3d, the scattered and transmitted light are all shown as a dipole-like intensity variation in a polar graph when an HWP was used to adjust the incident polarization relative to the boundary of the two asymmetric slits. The maximum light intensity is observed at the incident polarization of 90° and 270°, and the minimum light corresponds to the incident polarization of 0° and 180°. From the optical images in Figure 3e, a clear maximum transmitted bright spot was observed only if the incident polarization was perpendicular to the boundary of the two asymmetric slits, as indicated by the green arrows. When the incident polarization was rotated by 90° through HWP, the intensity of the light spot at the apex disappeared because of the internally coupling of incident beam and nanofocusing by SPP mode, resulting in background free of light. These observations imply that the light spot is indeed related to the coupling of the incident mode and the asymmetric slits, and originated from the far-field emission of the circumference interference plasmon nanofocus spot, which is also verified by the same dipole-like intensity variation and electric field distributions of the simulation results (Supplementary Figure S6).

2.4 Broadband plasmon nanofocusing

The broadband property of plasmon nanofocusing was experimentally analyzed through coupling broadband linearly polarized light to the optical fiber. Figure 4a shows the transmitted light spots in the vicinity of the apex of the asymmetric fiber tip over the wavelength range of 500–800 nm. The white lines indicate the outer shape of the two semicircular slits. These images visually confirm full optical wavelengths plasmon nanofocusing of the asymmetric fiber tip. Because of optical fiber propagation loss and far-field scattering efficiency at different wavelengths [32], the transmitted light intensity is much lower at longer wavelength in the visible spectrum, and hence, the incident power was increased by dozens of times to improve the transmitted intensity of the asymmetric fiber tip, as shown in Figure 4a. To further elucidate the broadband property, the phase delay of the excited SPP waves on the opposing facets was calculated by varying the asymmetric degree H of the two asymmetric slits based on Eq. (1), as shown in Figure 4b. Near H = 935 nm, the phase delay is nearly equal to π in the full visible wavelength range. Considering the slit width, the deviation error is only 3.2% related to phase π in the wavelength range of 530–800 nm, indicating that the constructive interference of the SPP waves will be achieved over a wide wavelength range.

The electric field distribution and enhancement near the apex at multiple excitation wavelengths were then simulated to validate broadband plasmon interference nanofocusing. Figure 4c shows that the E intensity enhancement spectrum varies with different asymmetric degrees H. Near H = 935 nm, the near field enhancement is maximum, which agrees well with the calculation. Versus the one-side plasmonic excitation (also see Supplementary Figure S9), the circumference interference method has more than two fold E intensity enhancement. To verify that the plasmonic nanofocusing is associated with constructively circumference interference, the E_z phase distribution near the apex of one-side plasmonic nanofocusing and circumference interference were investigated and compared. As shown in Figure 4e, the E_z phase distribution of the circumference interference is the same on the opposing facets for the longer wavelength range. In the shorter wavelength range, SPP waves are submerged by weak incident light transmitted through subwavelength slits [46] because of the enormous propagation loss. Therefore, the phase below the apex is the same, and the phase of the other areas is opposite. Within the same broadband wavelength, the E_z phase distribution is reversed on the opposing facets, and the phase below the apex is same for one-side plasmon propagation and mode evolution (Supplementary S8). These reversal phase distributions are further evidence that the asymmetric fiber tip with two slits can form a nanoscale spot with enhanced electric field intensity over a wide wavelength range because the constructive interference of SPP waves occurs around the entire solid circumference of the cone.

In the spectral experiment, there is a substantial decrease in transmitted intensity at longer wavelengths, which is contrary to the simulation results, as shown in Figure 4a and c. These opposite results are mainly caused

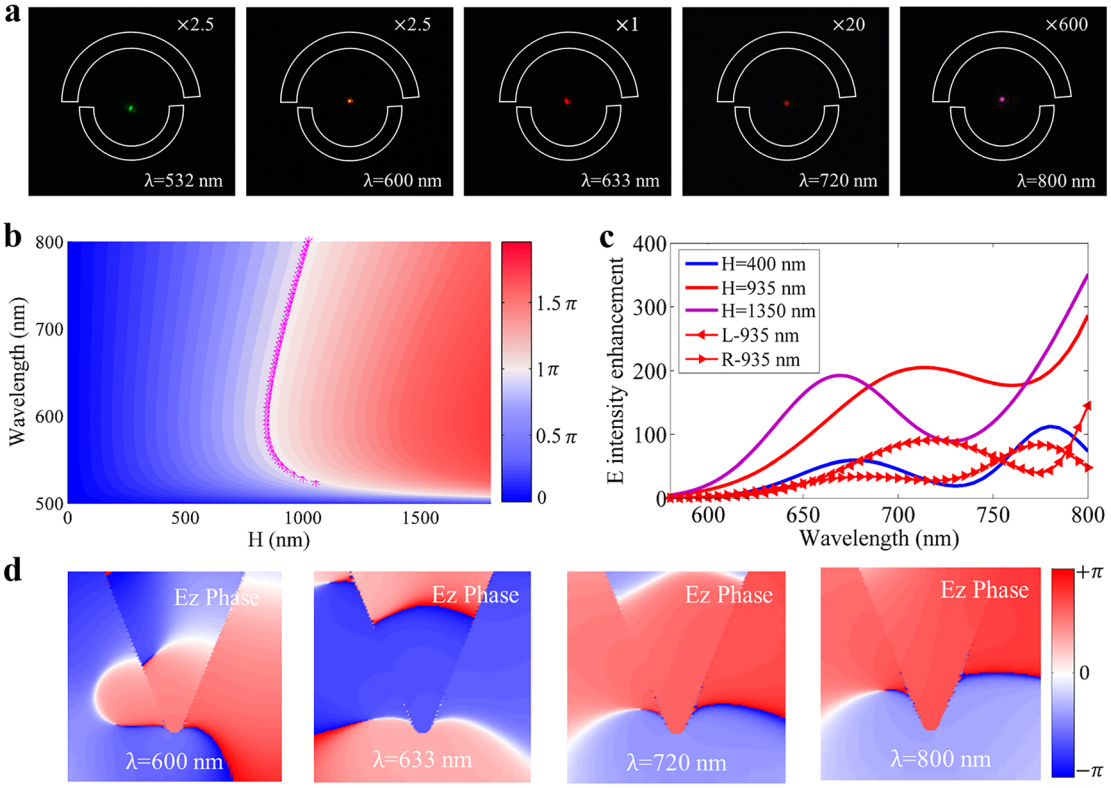

Figure 4: Broadband property of plasmon nanofocusing.
(a) Optical images of the forward-transmitted light of the asymmetric fiber tip over the broadband wavelength range. The numbers in the upper right corner of the images represent the multiple of the incident power relative to the incident power at the wavelength of 633 nm. (b) Calculated phase delay of the SPP waves on the opposing facets of the asymmetric fiber tip varying with asymmetric degree *H* and wavelength. The pink points mark the π phase delay positions. (c) Simulated *E* intensity enhancement spectrum at different asymmetric degrees *H*. For one-side plasmons nanofocusing, only one slit was etched corresponding to the position where *H* = 935 nm as indicated by L-935 and R-935, respectively. (d) E_z phase maps in the vicinity of the apex with asymmetric degree *H* = 935 nm. The coordinate of (d) is the same as that in Figure 2.

to wavelength-dependent fiber transmission and coupling efficiency. For the real optical fiber, the cutoff wavelength and working wavelength range are more important, which cause a certain deviation in transmitted light intensity with the simulation. The relative coupling efficiency of the optical fiber used in experiment at different incident wavelength was tested (see Supplementary Figure S8), and it is found that the coupling efficiency at near-infrared wavelengths is much lower than that at the wavelength of 600 nm. So, in the transmitted spectrum, the transmitted light intensity is much lower at longer wavelength with the same incident power, and higher incident power was used to obtain the transmitted spectrum at near-infrared wavelengths, as shown in Figure 5a. In experiment, the incident power of a wavelength of 800 nm should increase by hundreds of times than that of a wavelength of 633 nm to obtain a nearly equal transmitted intensity. Further, the effect of the spectral response of experimental device on the transmitted spectrum was investigated. At the wavelength range of 600–720 nm, the transmitted intensity starts to decrease and the incident power starts to increase, marked as the shaded area in Figure 5a. The relative enhancement of these turning points relative to that at the wavelength of 600 nm was calculated and compared with the numerical simulations. As shown in Figure 5b, the trend of relative enhancement is opposite to the trend of relative coupling efficiency. It is this opposite trend that leads to a substantial decrease in the transmitted light intensity at long wavelengths. So the relative coupling efficiency was used to compensate the transmitted light intensity. Considering the spectral response of the experimental device, the experimentally relative enhancement, defined as the product of relative transmission efficiency and relative coupling efficiency (Supplementary S7), is higher at longer wavelengths and its qualitative tendency is consistent with the simulation results. These results

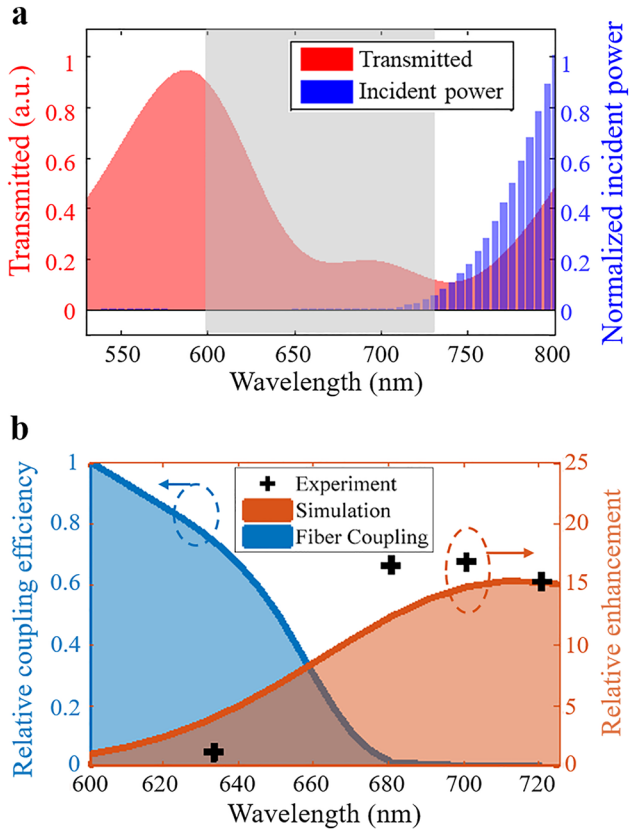

Figure 5: Spectral response and analysis.
(a) Transmitted spectrum of the optical spot at the apex of the asymmetric fiber tip and the corresponding normalized incident power. The red area indicates the transmitted intensity in visible wavelengths, and the blue bars represent the normalized incident power. (b) The relative coupling efficiency of the experimental device, and the relative electric field enhancement at the turning points considering the spectral response of experimental device compared with simulation. The blue area indicates the relative coupling efficiency of the optical fiber. The brown area indicates the relative enhancement of the simulation results. The black crosses indicate the relative enhancement of the experiment results.

further demonstrate that the experiment results are correct and the transmitted spectrum is significantly affected by the spectral response of the single-mode optical fiber.

3 Conclusions

The asymmetric fiber tip that was fabricated by standard processing technologies can create broadband nanoscale light source at the nanotip with 10 nm apex, which has the potential to replace aperture fiber tip to improve the resolution of scanning near-field optical microscopy. The broadband interference nanofocusing property within the full optical wavelengths of the optical fiber provides a high freedom of wavelength at the nanoscale, which is promising for multiple applications in all fields of plasmonics. Because of constructive SPP interference around the entire solid circumference of the cone, the electric field intensity of asymmetric fiber tip is two times than that of nanofocusing through plasmon propagation, which can also be expected to have twice focusing efficiency. The coupling efficiency of the asymmetric fiber tip is estimated to be about 0.2–2% in visible wavelengths. This coupling efficiency is a few times lower than the grating resonance plasmonic probes designed to couple a particular wavelength (typically 10%), but it is much higher than the aperture-type tips (typically 0.001–0.01%). The coupling efficiency in this structure is high enough for experimental observations, and the near-field measurement applications of this asymmetric fiber tip are now studying. With proper optimization, this three-dimensional plasmonic modulation and nanofocusing method can be extended to the design of near-infrared band fiber, which offers new scheme for broadband nanofocusing and plasmon modulation of functional elements.

In conclusion, an asymmetric fiber tip for deep subwavelength broadband interference nanofocusing of light was implemented and experimentally characterized. By introducing π phase delay to the SPP waves on the opposing facets, plasmonic polarization is reversed and the linearly polarized SPP mode is converted to the radially polarized SPP mode when the linearly polarized beam couples to the two asymmetric semicircular slits, allowing constructive interference and a nanoscale spot at the nanotip with 10 nm apex. By performing a detailed spectral and polarization analysis of the transmitted and scattered light, the scattered light is unambiguously originated from the longitudinally polarized SPP nanofocusing at the tip apex. Combined with detailed calculation and simulation, the experiments demonstrate the broadband nanofocusing property of the asymmetric fiber tip within the full optical wavelengths, resulting from constructive interference of the SPP waves at any two antipodal points of the circumference of the cone over a wide wavelength range. Because of the broadband plasmon nanofocusing on a flexible fiber platform, this asymmetric fiber tip with broadband interference nanofocusing will have more applications in near-field imaging, nanolithography, Raman spectroscopy, and sensing of chemical or biological processes.

4 Methods

4.1 Finite-difference time-domain simulation methods

In the simulation, for the symmetric fiber tip, the thickness of the Au film was set as 50 nm. For the asymmetric fiber tip, the thickness of the Au film was set as 180 nm. The slit width was set as 120 nm, and the slit depth ratio was set as 1 (Supplementary S5). The computation window was enclosed by a perfectly matched layer (PML) to avoid any artificial reflection from the boundaries. Near the tip apex, the grid sized was set as 2 nm to ensure simulation accuracy. The 3D FDTD, lumerical method was employed to visually investigate the internal illumination process via HE_{11} and TM_{01}. The optical vector modes TM_{01} and HE_{11} were selected using the Mode Source function. The dispersion of the dielectric function of Au was taken from Johnson and Christy. The SiO_2 is a dielectric with permittivity $\varepsilon_1 = 2.12$. To calculate the local field enhancement, the E field intensity factor was defined as the ratio between the localized E field intensity located 3 nm below the tip apex and the E field intensity of the incident light.

4.2 Asymmetric probe fabrication and spectral measurement

In the experiment, the single-mode optical fiber (Nufern, 630-HP) was etched using tube-etching method first using a dip coater (SYDC-100), and the tapered fiber with cone angle of 32° was obtained. Then the tapered fiber was evaporated by 10 nm Cr and 180 nm Au to obtain a chemically stable metal film by using an electron beam evaporation coating machine (HHV, TF500). Finally, the metallic tapered fiber was processed using focus ion beam (FIB, Helios Nanolab 6600) to fabricate two asymmetric slits, as shown in S2. In the FIB process, the Ga ion beam was facing the tip apex, and the processing parameters were 20 pA and 30 kV. On the tip side, the width and depth of the two slits were approximately 120 and 180 nm, respectively.

In the spectral measurement experiments, a broadband white light supercontinuous light source (Leukos, AUT-ROCK) was used as the incident laser. A color high-definition scientific CMOS camera (Thorlabs, CS126CU) was used to image the far-field light spot from the tip apex of the asymmetric fiber tip. In Figure 3a, LP_1 was used to ensure the linear polarization of the incident laser and was placed between an attenuator (A) and a half waveplate (HWP). LP_2 was used to extract the longitudinally polarized electric field and the transversely polarized electric field from the side-scattered light, and was placed in front of the CMOS camera. To investigate the dominant electric field component of the side-scattered light, the LP_1 between A and HWP was fixed, and only the LP_2 was adjusted. In Figure 3b, when the white arrow is horizontal, i. e. the LP_2 is parallel to the tip axis, the longitudinally polarized electric field is obtained. Similarly, when the white arrow is vertical, i. e. the LP_2 is perpendicular to the tip axis; the transversely polarized electric field is obtained.

Supporting information

The Supporting Information is available free of charge. Details on the design of slit etching direction and the fabrication of the asymmetric fiber tip, the nanofocusing characteristics of the radially polarized mode and linearly polarized mode, and the plasmons propagation and phase distribution on the opposing facets of one side plasmons nanofocusing (PDF).

Author contribution: S. Yang initiated the idea and the research topic. S. Li fabricated and characterized the probe, developed the modeling and analyzed the data. F. Wang performed the nanofocusing experiments. Q. Liu established the experiment setup. B. Cheng contributed to discussion of the results. Y. Rosenwaks contributed to discussion. S. Yang and S. Li wrote up the manuscript.
Research funding: The research was funded by the Program for Science and Technology Innovation Group of Shaanxi Province (2019TD-011), the Key Research and Development Program of Shaanxi Province (2020ZDLGY04-02), and the Fundamental Research Funds for the Central Universities.
Conflict of interest statement: The authors declare no competing financial interests.

References

[1] W. L. Barnes, A. Dereux, and T. W. Ebbesen, "Surface plasmon subwavelength optics," *Nature*, vol. 424, pp. 824–830, 2003.
[2] M. I. Stockman, "Nanofocusing of optical energy in tapered plasmonic waveguides," *Phys. Rev. Lett.*, vol. 93, p. 137404, 2004.
[3] H. Shen, G. Lu, Y. He, Y. Cheng, H. Liu, and Q. Gong, "Directional and enhanced spontaneous emission with a corrugated metal probe," *Nanoscale*, vol. 6, pp. 7512–7518, 2014.
[4] F. Lu, W. Zhang, M. Liu, et al., "Grating-assisted coupling enhancing plasmonic tip nanofocusing illuminated via radial vector beam," *Nanophotonics*, vol. 8, pp. 2303–2311, 2019.
[5] C. Ropers, C. C. Neacsu, T. Elsaesser, et al., "Grating- coupling of surface plasmons onto metallic tips: a nanoconfined light source," *Nano Lett.*, vol. 7, pp. 2784–2788, 2007.
[6] W. Bao, M. Melli, N. Caselli, et al., "Mapping local charge recombination heterogeneity by multidimensional nanospectroscopic imaging," *Science*, vol. 338, pp. 1317–1321, 2012.
[7] M. Liu, F. Lu, W. Zhang, and L. Huang, "Highly efficient plasmonic nanofocusing on a metallized fiber tip with internal illumination of the radial vector mode using an acousto-optic coupling approach," *Nanophotonics*, vol. 8, pp. 921–929, 2019.
[8] D. K. Gramotnev and S. I. Bozhevolnyi, "Plasmonics beyond the diffraction limit," *Nat. Photonics*, vol. 4, pp. 83–91, 2010.
[9] R. Eckert, J. M. Freyland, H. Gersen, et al., "Near-field fluorescence imaging with 32 nm resolution based on microfabricated cantilevered probes," *Appl. Phys. Lett.*, vol. 77, pp. 3695–3697, 2000.
[10] T. Sondergaard, S. I. Bozhevolnyi, J. Beermann, S. M. Novikov, E. Devaux, and T. W. Ebbesen, "Resonant plasmon nanofocusing by closed tapered gaps," *Nano Lett.*, vol. 10, pp. 291–295, 2010.

[11] H. Choo, M. Kim, M. Staffaroni, et al., "Nanofocusing in a metal-insulator-metal gap plasmon waveguide with a three-dimensional linear taper," *Nat. Photonics*, vol. 6, pp. 838–844, 2012.
[12] A. Tuniz, O. Bickerton, F. J. Diaz, et al., "Modular nonlinear hybrid plasmonic circuit," *Nat. Commun.*, vol. 11, p. 2413, 2020.
[13] T. Zhang, M. Wang, Y. Yang, et al., "An on-chip hybrid plasmonic light steering concentrator with ~ 96% coupling efficiency," *Nanoscale*, vol. 10, pp. 5097–5104, 2018.
[14] Z. Cai, Y. Xu, C. Wang, and Y. Liu, "Polariton photonics using structured metals and 2D materials," *Adv. Opt. Mater.*, vol. 8, p. 1901090, 2020.
[15] L. Li, S. Wang, S. Zhu, and X. Zhang, "Broad band focusing and demultiplexing of in-plane propagating surface plasmons," *Nano Lett.*, vol. 11, pp. 4357–4361, 2011.
[16] J. Yang, S. Zhou, C. Hu, W. Zhang, X. Xiao, and J. Zhang, "Broadband spin-controlled surface plasmon polariton launching and radiation via L-shaped optical slot nanoantennas," *Laser Photon. Rev.*, vol. 8, pp. 590–595, 2014.
[17] X. Yin, T. Steinle, L. Huang, et al., "Beam switching and bifocal zoom lensing using active plasmonic metasurfaces," *Light Sci. Appl.*, vol. 6, 2017, Art no. e178016.
[18] S. Kawata, Y. Inouye, and P. Verma, "Plasmonics for near-field nano-imaging and superlensing," *Nat. Photonics*, vol. 3, pp. 388–394, 2009.
[19] S. F. Becker, M. Esmann, K. W. Yoo, et al., "Gap-plasmon-enhanced nanofocusing near-field microscopy," *ACS Photonics*, vol. 3, pp. 23–32, 2016.
[20] D. Sadiq, J. Shirdel, J. S. Lee, E. Selishcheva, N. Park, and C. Lienau, "Adiabatic nanofocusing scattering- type optical nanoscopy of individual gold nanoparticles," *Nano Lett.*, vol. 11, pp. 1609–1613, 2011.
[21] R. H. Jiang, T. J. Yen, C. Chen, D. Z. Lin, H. C. Chou, and J. Y. Chu, "Near-field plasmonic probe with super resolution and high throughput and signal-to-noise ratio," *Nano Lett.*, vol. 18, pp. 881–885, 2018.
[22] H. W. Kihm, J. Kim, S. Koo, et al., "Optical magnetic field mapping using a subwavelength aperture," *Opt. Express*, vol. 21, pp. 5625–5633, 2013.
[23] C. C. Neacsu, G. A. Reider, and M. B. Raschke, "Second-harmonic generation from nanoscopic metal tips: symmetry selection rules for single asymmetric nanostructures," *Phys. Rev. B*, vol. 71, p. 201402, 2005.
[24] V. Kravtsov, R. Ulbricht, J. M. Atkin, and M. B. Raschke, "Plasmonic nanofocused four-wave mixing for femtosecond near-field imaging," *Nat. Nanotechnol.*, vol. 11, pp. 459–464, 2016.
[25] C. Chen, N. Hayazawa, and S. Kawata, "A 1.7nm resolution chemical analysis of carbon nanotubes by tip-enhanced Raman imaging in the ambient," *Nat. Commun.*, vol. 5, p. 3312, 2014.
[26] S. Jiang, Y. Zhang, R. Zhang, et al., "Distinguishing adjacent molecules on a surface using plasmon-enhanced Raman scattering," *Nat. Nanotechnol.*, vol. 10, pp. 865–869, 2015.
[27] B. N. Tugchin, N. Janunts, A. E. Klein, et al., "Plasmonic tip based on excitation of radially polarized conical surface plasmon polariton for detecting longitudinal and transversal fields," *ACS Photonics*, vol. 2, pp. 1468–1475, 2015.
[28] F. Lu, W. Zhang, L. Zhang, M. Liu, and T. Mei, "Nanofocusing of surface plasmon polaritons on metal-coated fiber tip under internal excitation of radial vector beam," *Plasmonics*, vol. 14, pp. 1593–1599, 2019.
[29] Y. Wang, W. Srituravanich, C. Sun, and X. Zhang, "Plasmonic nearfield scanning probe with high transmission," *Nano Lett.*, vol. 8, pp. 3041–3045, 2008.
[30] Y. Wang, Y. Y. Huang, and X. Zhang, "Plasmonic nanograting tip design for high power throughput near-field scanning aperture probe," *Opt. Express*, vol. 18, pp. 14004–14011, 2010.
[31] C. C. Neacsu, S. Berweger, R. L. Olmon, L. V. Saraf, C. Ropers, and M. B. Raschke, "Near-field localization in plasmonic superfocusing: a nanoemitter on a tip," *Nano Lett.*, vol. 10, pp. 592–596, 2010.
[32] N. C. Lindquist, P. Nagpal, A. Lesuffleur, D. J. Norris, and S. H. Oh, "Three-dimensional plasmonic nanofocusing," *Nano Lett.*, vol. 10, pp. 1369–1373, 2010.
[33] S. Cherukulappurath, T. W. Johnson, N. C. Lindquist, and S. H. Oh, "Template-stripped asymmetric metallic pyramids for tunable plasmonic nanofocusing," *Nano Lett.*, vol. 13, pp. 5635–5641, 2013.
[34] T. Umakoshi, Y. Saito, and P. Verma, "Highly efficient plasmonic tip design for plasmon nanofocusing in near-field optical microscopy," *Nanoscale*, vol. 8, pp. 5634–5640, 2016.
[35] T. Umakoshi, M. Tanaka, Y. Saito, and P. Verma, "White nanolight source for optical nanoimaging," *Sci. Adv.*, vol. 6, p. 4179, 2020.
[36] K. Zhang, S. Taniguchi, and T. Tachizaki, "Generation of broadband near-field optical spots using a thin-film silicon waveguide with gradually changing thickness," *Opt Lett.*, vol. 43, pp. 5937–5940, 2018.
[37] X. Piao, S. Yu, and N. Park, "Control of fano asymmetry in plasmon induced transparency and its application to plasmonic waveguide modulator," *Opt. Express*, vol. 20, pp. 18994–18999, 2012.
[38] Q. Qian, H. Yu, P. Gou, J. Xu, and Z. An, "Plasmonic focusing of infrared SNOM tip patterned with asymmetric structures," *Opt. Express*, vol. 23, pp. 12923–12934, 2015.
[39] V. Lotito, U. Sennhauser, C. Hafner, and G. Bona, "Fully metal-coated scanning near-field optical microscopy probes with spiral corrugations for superfocusing under arbitrarily oriented linearly polarized excitation," *Plasmonics*, vol. 6, pp. 327–336, 2011.
[40] J. Li, J. Mu, B. Wang, et al., "Direct laser writing of symmetry-broken spiral tapers for polarization-insensitive three-dimensional plasmonic focusing," *Laser Photon. Rev.*, vol. 8, pp. 602–609, 2014.
[41] S. Li and S. Yang, "Nanofocusing of a novel plasmonic fiber tip coupling with nanograting resonance," *J. Phys. Appl. Phys.*, vol. 53, p. 21510, 2020.
[42] S. Kim, N. Yu, X. Ma, et al., "High external-efficiency nanofocusing for lens-free near-field optical nanoscopy," *Nat. Photonics*, vol. 13, pp. 636–643, 2019.
[43] A. Bouhelier, J. Renger, M. R. Beversluis, and L. Novotny, "Plasmon- coupled tip- enhanced near- field optical microscopy," *J. Microsc.*, vol. 210, pp. 220–224, 2002.

[44] Y. Wu, L. Lu, Y. Chen, et al., "Excitation and analyzation of different surface plasmon modes on a suspended Ag nanowire," *Nanoscale*, vol. 11, pp. 22475–22481, 2019.
[45] N. A. Janunts, K. S. Baghdasaryan, K. V. Nerkararyan, and B. Hecht, "Excitation and superfocusing of surface plasmon polaritons on a silver-coated optical fiber tip," *Opt Commun.*, vol. 253, pp. 118–124, 2005.
[46] B. Hecht, B. Sick, and U. P. Wild, "Scanning near-field optical microscopy with aperture probes: fundamentals and applications," *J. Chem. Phys.*, vol. 112, pp. 7761–7774, 2000.

Supplementary Material: The online version of this article offers supplementary material (https://doi.org/10.1515/nanoph-2021-0405).